Photorefractive crystals for the stabilization of the holographic setup

Alexei A. Kamshilin, Jaime Frejlich, and Lucila Cescato

A photorefractive crystal of the sillenite family in a two-wave mixing experiment is used as a fundamental component in a negative feedback system for stabilizing a holographic setup. The behavior of such a stabilization system is theoretically analyzed, and the advantages and limitations of using a real-time nonpermanent recording material (photorefractive crystal) are discussed. We present experimental results using a $Bi_{12}TiO_{20}$ crystal, compare actual and predicted performances, and discuss the optimization of relevant parameters for better performance of the whole stabilizing system. Theoretical analysis and experimental results show this system to have interesting perspectives for further development.

I. Introduction

Stabilization of a holographic setup is needed to achieve high-contrast holographic fringes for long-time exposure experiments. Some active stabilization methods have already been proposed[1,2] using basically a piezoelectric mirror (or any other phase shifting mechanism) in one of the arms of the setup and an adequate electronics and detection system. These elements form a negative feedback system which compensates for disturbances in the holographic setup by driving the piezoelectric mirror to keep constant the optical path length difference between both arms in the setup. The piezoelectric mirror is usually activated by the variation of intensity (arising from perturbations on the phase difference of the interfering beams) at a fixed area of the holographic interference pattern which is projected onto a detector. The SNR at this detection step is one of the critical parameters limiting the performance of the feedback system. The interference pattern must be spatially magnified to allow for detection of intensity variations on a dimension comparable to the pattern period. Such magnification may be achieved using a microscope objective[1] in which case a corresponding decrease of light intensity at the detector occurs thus lowering the sensitivity of the stabilization system.

Johansson *et al.*[3] employed an efficient method for spatial amplification of the interference pattern by mixing the two interfering beams in the holographic setup using an auxiliary grating previously recorded in this setup. This wave mixing is comparable to the formation of moirelike fringes of a large period, and it arises from the interference of one of the transmitted beams with its holographic reconstruction by the second beam as is schematically described in Fig. 1. A much higher intensity is available compared to the above referenced method. MacQuigg[2] further improved this method by producing a high-frequency low-amplitude phase oscillation in one of the interfering beams, which may be produced by an oscillation at the piezoelectric mirror. A lock-in amplifier tuned to this frequency is employed in the detection system thus increasing considerably the SNR. The large spatial period amplification and high intensity resulting in this moirelike pattern allow a further increase in the SNR by concentrating light on the detector from a large interference pattern area, the size of which depends on the moirelike structure period available. This much stronger signal allows also using PIN diodes for detection which are less sensitive but much faster than the usual planar-type Si detectors. This fast response is fundamental for detection of the high-frequency phase oscillation and also reduces the delay of the stabilization feedback loop. This allow further amplification in the stabilization system without the occurrence of oscillations,[4] which results in better sensitivity of the system. Unfortunately, this method requires that a new auxiliary grating be produced each time the setup configuration is changed. Another limitation arises from the fact that the period of the moirelike pattern (which limits the size of the area where

Alexei A. Kamshilin is with Academy of Sciences of the U.S.S.R., A. F. Ioffe Physico-Technical Institute, 194021 Leningrad, U.S.S.R.; the other authors are with Universidade Estadual de Campinas, Instituto de Fisica, Laboratorio de Optica, Caixa Postal 6165, 13100 Campinas, SP, Brazil.

Received 11 December 1985.
0003-6935/86/142375-07$02.00/0.

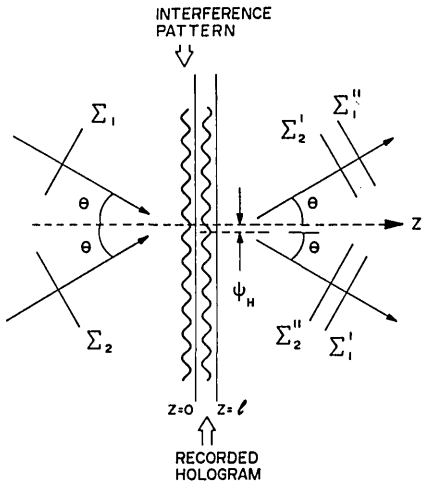

Fig. 1. Two-wave mixing. Waves Σ_1 and Σ_2 interfere producing an interference pattern and a volume grating in the recording material of thickness l. Because of the recording mechanism or any other reasons the recorded grating may be phase shifted ψ_H relative to the interference pattern. $\Sigma_1''(\Sigma_2'')$ is the diffraction of $\Sigma_1(\Sigma_2)$ by the volume grating (hologram), which may also be thought of as being the holographic reconstruction of $\Sigma_2(\Sigma_1)$ using $\Sigma_1(\Sigma_2)$ as a reference.

light may be collected to be concentrated on the detector) is limited by the mechanical adjustments available and the deformation of the wave front reconstructed at the auxiliary grating due to changes in the recording material during developement.

We discuss the possibility of using photorefractive crystals as auxiliary elements substituting the auxiliary grating in the feedback stabilization system. We present also some preliminary experimental results using a $Bi_{12}TiO_{20}$ (BTO) crystal of the sillenite family ($Bi_{12}SiO_{20}$-type). Among the photorefractive crystals that are widely used for reversible real-time recording of holograms,[5] those of the sillenite family show the best sensitivity.[6] The use of photorefractive crystals in active stabilization systems does not suffer from the limitations referred to above: (a) it is not necessary to prepare a new control grating each time the holographic configuration is changed because the new interference pattern is recorded in real time; (b) the area where light may be collected from for detection is only limited by the crystal size because there is no deformation of the real-time holographic wave front reconstructed compared to the transmitted one so that no interference fringes appear in the field of view during beam mixing.

II. Theoretical Analysis

We have used the typical transverse[7] electrooptic (110) orientation of the BSO-type cubic crystal with the holographic vector $\mathbf{K}$ ($|\mathbf{K}| = 2\pi/\Delta$, with Δ being the period of fringes) parallel to $[1\bar{1}0]$ as shown in Fig. 2. Writing the crystal dielectric tensor in principal axes x, y, z we have

$$\hat{\epsilon} = \begin{vmatrix} \epsilon_0 + \Delta\epsilon & 0 & 0 \\ 0 & \epsilon_0 - \Delta\epsilon & 0 \\ 0 & 0 & \epsilon_0 \end{vmatrix} = \epsilon_0 + \Delta\hat{\epsilon}, \tag{1}$$

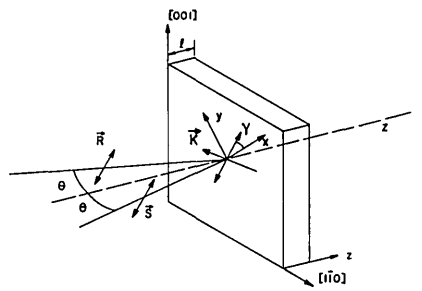

Fig. 2. Typical transverse electrooptic configuration of the $Bi_{12}TiO_{20}$ (BTO) sample. Incident beams are linearly polarized with angle $\gamma = \gamma_0$ measured from the x axis. x, y, and z are the principal axes, and $\mathbf{K}$ is the grating vector.

where ϵ_0 is the isotropic dielectric constant, and $\Delta\epsilon$ is its change via electrooptic effect produced by holographic recording assuming an electric field $\mathbf{E}$ parallel to $[1\bar{1}0]$, where $\Delta\epsilon = n_0^4 r_{41} E$ as deduced from the refractive-index variation, $\Delta n = n_0^3 r_{41} E/2$, already reported elsewhere.[7] r_{41} is an electrooptic coefficient ($r_{41} = r_{52}$), and n_0 is the isotropic index of refraction of the crystal.

In the case of holographic recording without an external electric field, a steady-state space-charge internal field E_{sc} distribution arises due to hologram recording.[6,8] Let the holographic pattern projected on the crystal be described by the intensity modulation

$$I(r) = I_0(1 + m\cos\mathbf{K}\cdot\mathbf{r}), \tag{2}$$

where m is the visibility of the interference pattern fringes. If we assume a pure diffusion mechanism for recording, the space-charge electric field E_{sc} is represented by[6]

$$\mathbf{E}_{sc}(r) = m\mathbf{E}_{sc}^0 \sin(\mathbf{K}\cdot\mathbf{r}), \tag{3}$$

which is $\pi/2$ phase-shifted relative to the interference pattern.

Evaluating the intensity of the mixed beams after the crystal, using Kogelnik's coupled-wave theory[9] applied to the anisotropic case,[10] for a sinusoidal nonabsorbing phase grating and for perfect Bragg conditions, we get the following equations:

$$\left.\begin{aligned} \frac{dR(z)}{dz} &= -i(\Gamma\cdot\hat{\chi}\mathbf{s})S(z), \\ \frac{dS(z)}{dz} &= -i(\mathbf{s}\cdot\hat{\chi}\Gamma)R(z), \end{aligned}\right\} \tag{4}$$

where $R(z)$ and $S(z)$ are described in Fig. 3 and represent the amplitude of waves propagating along the direction of incident waves Σ_1 and Σ_2 (Fig. 1), respectively. R and S may be conventionally labeled as reference and signal beams, respectively, and their polarization directions relative to the x axis in Fig. 2 are represented by unit vectors Γ and $\mathbf{s}$, respectively:

$$\mathbf{R}(z) = R(z)\Gamma; \tag{5}$$

$$\mathbf{S}(z) = S(z)\mathbf{s}. \tag{6}$$

The tensor $\hat{\chi}$ in Eq. (4) is the coupling wave tensor which is described by

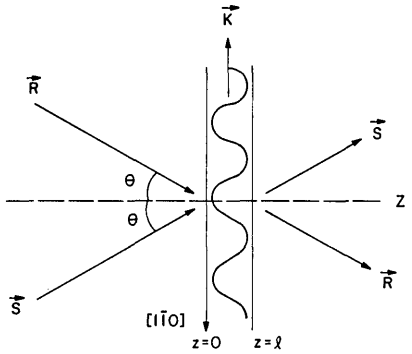

Fig. 3. Wave mixing using a BTO sample in a transverse electrooptic configuration. According to Fig. 1, $R(S)$ for $z > 0$ is the sum of the transmitted wave $\Sigma_1'(\Sigma_2')$ and the diffracted $\Sigma_2''(\Sigma_1'')$. According to coupled-wave theory, the latter arises from energy exchange from $\Sigma_2'(\Sigma_1')$ as it goes through the volume grating.

$$\hat{\chi} = \frac{m\pi n_0^3 r_{41} E_{sc}^0}{2\lambda \cos\theta} \begin{vmatrix} 1 & 0 & 0 \\ 0 & -1 & 0 \\ 0 & 0 & 0 \end{vmatrix}, \tag{7}$$

where 2θ is the angle between propagation vectors of R and S inside the crystal. The coupling between reference and signal beams is determined by the scalar product $(\Gamma \cdot \hat{\chi}\mathbf{s})$, which depends on the polarization of both beams. It achieves the maximum value $\Gamma \cdot \hat{\chi}\mathbf{s} = \chi = m\pi n_0^3 r_{41} E_{sc}^0/(2\lambda \cos\theta)$ when the angles of Γ and $\mathbf{s}$ relative to the x axis are symmetric (that means $+\gamma$ and $-\gamma$, respectively in Fig. 2). This means that there is diffraction with rotation of the polarization plane as observed earlier.[11,12]

Because of such a wave-coupling effect in anisotropic media, Σ_2'' and Σ_1'' in Fig. 1 represent $-\gamma$ polarization direction waves coupled to Σ_2' and Σ_1' waves, respectively, the latter in their turn representing the transmission of incident waves Σ_2 and Σ_1 (both having a $+\gamma$ linear polarization direction as seen in Fig. 2), respectively. Wave Σ_2'' (and similarly for Σ_1'') may be thought of as arising either from diffraction of Σ_2 or as an holographic reconstruction of wave Σ_1 using Σ_2 as a reference. In any case there is a rotation of polarization from $+\gamma$ to $-\gamma$.

The coupled differential equations in Eq. (4) may be solved with boundary conditions:

$$\left.\begin{aligned} R_\gamma(0) &= R_0, \\ S_\gamma(0) &= S_0 \exp[i(\Phi + \psi_H)], \\ R_{-\gamma}(0) &= 0, \\ S_{-\gamma}(0) &= 0, \end{aligned}\right\} \tag{8}$$

where the subscripts γ and $-\gamma$ represent the linear polarization direction angles. If the hologram recorded in the crystal is $-\psi_H$ phase shifted along the $\mathbf{K}$ grating vector direction, relative to the interference pattern it is obviously equivalent from all points of view to an opposite phase shift $(+\psi_H)$ in the interference pattern. Thus we introduced the ψ_H in Eq. (8). The Φ phase in these equations accounts for random and/or purposely induced perturbations in the holographic setup.

For a purely diffusion recording mechanism $\psi_H = \pi/2$ as was already mentioned, in which case the solution of Eq. (4) with boundary conditions in Eq. (8) is

$$\left.\begin{aligned} R_\gamma(z) &= R_0 \cos\chi z, \\ S_\gamma(z) &= S_0 \exp[i(\Phi + \pi/2)] \cos\chi z, \\ R_{-\gamma}(z) &= -iS_0 \exp[i(\Phi + \pi/2)] \sin\chi z, \\ S_{-\gamma}(z) &= -iR_0 \sin\chi z. \end{aligned}\right\} \tag{9}$$

From Eqs. (9) we may calculate the intensities of the I_R and I_S beams after the crystal (Fig. 3) to be

$$I_R = R_0^2 \cos^2(\chi z) + S_0^2 \sin^2(\chi z) + R_0 S_0 \sin(2\chi z) \cos\phi \cos(2\gamma), \tag{10}$$

$$I_S = R_0^2 \sin^2(\chi z) + S_0^2 \cos^2(\chi z) - R_0 S_0 \sin(2\chi z) \cos\phi \cos(2\gamma). \tag{11}$$

Because of optical activity[13] ρ of our crystal, the polarization angle γ continuously changes throughout the crystal thickness [$\gamma(z) = \gamma_0 + \rho z$ with $\gamma_0 = \gamma(0)$], and assuming that $\chi \cdot l \ll 1$ and $\chi \ll \rho$, the solution of Eq. (4) for a crystal of thickness l leads to

$$I_R \cong R_0^2 + S_0^2\eta + 2R_0 S_0 \sqrt{\eta} \cos(2\gamma_0 + \rho l) \cos\Phi \tag{12}$$

instead of Eq. (10). The diffraction efficiency η may be written as

$$\eta = \chi^2 \left(\frac{\sin\rho l}{\rho}\right)^2 = \eta_0 \cdot m^2 \tag{13}$$

with

$$m = \frac{2R_0 S_0}{R_0^2 + S_0^2} \tag{14}$$

$$\eta_0 = \left(\frac{\pi n_0^3 r_{41} E_{sc}^0}{2\lambda \cos\theta}\right)^2 \cdot \left(\frac{\sin\rho l}{\rho}\right)^2. \tag{15}$$

Let us write the phase perturbation Φ in Eq. (12) as

$$\Phi = \psi + \psi_d \sin\Omega t, \tag{16}$$

where ψ is a random and/or purposely induced phase shift introduced in the setup, and ψ_d is the constant amplitude of a controlled phase modulation of frequency Ω. Assuming $\psi_d \ll 1$ and substituting Eq. (16) into Eq. (12), we may write

$$I_R = I_R^0 - I_\Omega \sin\Omega t, \tag{17}$$

$$I_R^0 \equiv R_0^2 + S_0^2\eta + 2R_0 S_0 \sqrt{\eta} \cos(2\gamma_0 + \rho l) \cos\psi, \tag{18}$$

$$I_\Omega \equiv 2R_0 S_0 \sqrt{\eta}\psi_d \cos(2\gamma_0 + \rho l) \sin\psi. \tag{19}$$

The last term in Eq. (17) is time-modulated with frequency Ω and amplitude I_Ω. Note that $I_\Omega = -\psi_d(\partial I_R^0/\partial\psi)$, which means that it represents the derivative of the intensity of the nonmodulated interference pattern as a function of phase shift ψ. Thus the term I_Ω may be used for controlling (and consequently for stabilizing using a negative feedback setup) the position of the interference pattern: $I_\Omega = 0$ for a maximum of an interference fringe and increasingly negative or positive (or vice versa depending on electronics employed) at one side or the other of this maximum.

The results above show that photorefractive crystals may be used as phase sensitive detectors for transducing the phase variations ψ between both interfering beams in a holographic setup into intensity variations that may be converted into an electrical signal at an appropriate photodetector. We shall profit from these properties for operating an active stabilization system as will be described in the next section.

III. Experimental results

We used the experimental setup described in Fig. 4. The interference pattern was produced using the 514-nm line of an argon-ion laser whose beam was divided into two by the beam splitter *BS*. The piezoelectric mirror (PZT), is placed in one of them. The PZT is modulated by a sinusoidal signal of frequency Ω and amplitude v_d produced by an oscillator (OSC) and is also driven by the output of a high-voltage (HV) source which amplifies the dc output voltage of the lock-in amplifier that is tuned to frequency Ω. As described in Sec. II, the BTO crystal converts the phase changes in the holographic setup into intensity variations by wave mixing. These variations are converted into an electrical signal whose oscillatory term of frequency Ω is amplified by the lock-in amplifier thus completing the feedback loop. The block diagram of the complete system and feedback loop is described in Fig. 4(b). The ac term of frequency Ω (the dc and other harmonics are rejected by the following lock-in amplifier) at the output of the PIN diode is

$$v_\Omega = V_\Omega \sin\Omega t \qquad \text{with } V_\Omega \equiv K_p I_\Omega, \tag{20}$$

where K_p is a parameter characterizing the PIN diode, and I_Ω is the amplitude of the oscillating term of the intensity at the input of the PIN as described in Eqs. (17) and (19). The output V_Ω' of the lock-in is a dc signal proportional to the amplitude V_Ω in Eq. (20). Substituting I_Ω into Eq. (20) by its expression in Eq. (19) we get

$$V'_\Omega = K_l V_\Omega = 2\psi_d K_l K_p R_0 S_0 \sqrt{\eta}\cos(2\gamma_0 + \rho l)\sin\psi, \tag{21}$$

where K_l is the amplification of the lock-in.

The signal V_Ω' is amplified by the high-voltage source whose value $K_0 V_\Omega'$ is added to the control low-amplitude signal from the oscillator ($v_d \sin\Omega t$) and used for driving the piezoelectric. It is convenient to write the phase shift ψ that was introduced in Eq. (16) as

$$\psi = \psi_N + \psi_f, \tag{22}$$

$$\psi_f = K^0_{\mathrm{PZT}} K_0 V'_\Omega, \tag{23}$$

where the term ψ_N represents the random phase shift produced by noise and perturbations in the setup. The ψ_f term is the phase shift produced by the action of the piezoelectric mirror as represented by Eq. (23), where K^0_{PZT} is the overall voltage-to-phase piezoelectric conversion factor for low temporal frequencies. The high-frequency signal from the oscillator is also converted into a phase modulation at the PZT so that we may also write

$$\psi_d = K^\Omega_{\mathrm{PZT}} v_d, \tag{24}$$

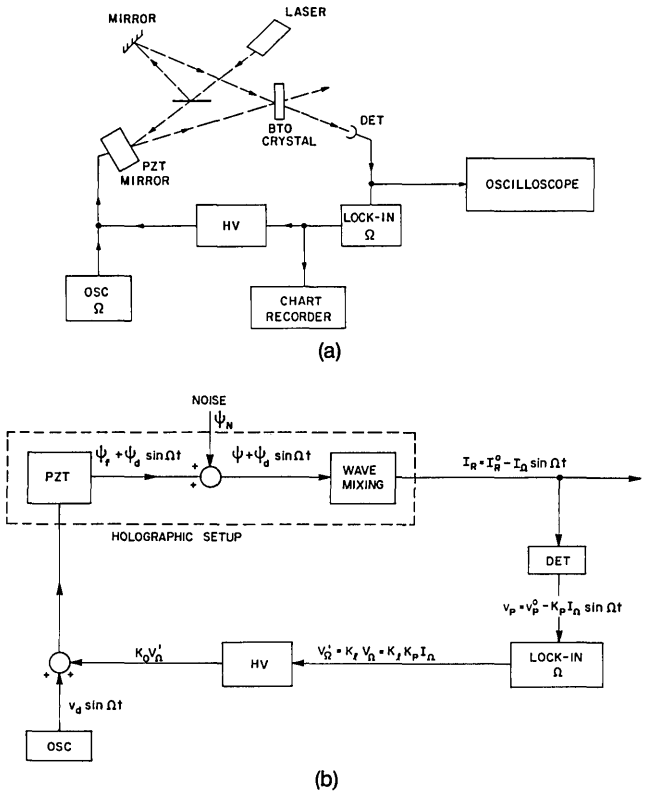

Fig. 4. (a) Holographic setup with negative feedback loop for stabilization. Wave mixing at the BTO crystal transduces a phase shift between both interfering beams into an intensity variation at the detector. The lock-in amplifier is tuned to frequency Ω at which the PZT is driven by the oscillator (OSC). The PZT is also driven by the high-voltage source (HV) which amplifies the lock-in output. (b) Flow chart illustrating the feedback loop operation.

where K^Ω_{PZT} has the same meaning as K^0_{PZT} but for frequency Ω. Substituting Eqs. (23) and (21) into Eq. (22) we get

$$\psi = \psi_N + K^0_{\mathrm{PZT}} K_0 2\psi_d K_l K_p R_0 S_0 \sqrt{\psi}\cos(2\gamma_0 + \rho l)\sin\psi, \tag{25}$$

which solution $\psi = 0$ (for $\psi_N = 0$) represents the stabilized system equilibrium position. Note that because of real-time recording properties of photorefractive crystals, the steady-state equilibrium position of the stabilized system should be necessarily reached at the nonperturbed ($\psi = 0$) open feedback loop equilibrium position of the holographic setup. For this position to represent a stable equilibrium the derivative $(\partial\psi_f/\partial\psi_N)$ should be negative, where the ideal situation should be $(\partial\psi_f/\partial\psi_N) = -1$. From Eqs. (25) and (22) we get

$$\left.\begin{aligned} &\partial\psi_f/\partial\psi_N = a\cos\psi/(1 - a\cos\psi), \\ &\text{with} \\ &\qquad a \equiv K^0_{\mathrm{PZT}} K_0 2\psi_d K_l K_p R_0 S_0 \sqrt{\eta}\cos(2\gamma_0 + \rho l). \end{aligned}\right\} \tag{26}$$

For our setup $|a| < 1$, which means that the equilibrium point $\psi = 0$ is stable for $a < 0$ (which signal is controlled at the lock-in amplifier output) because $\partial\psi_f/\partial\psi_N = -|a|/(1 + |a|) < 0$, and the ideal situation may be approached only for $|a| \gg 1$.

The performance of our stabilization system using the BTO crystal was measured in an open feedback loop. In doing so, a single steplike pulse of low-amplitude V_s was applied at the input to the piezoelectric mirror driver. The nonstabilized response of the whole system to such a perturbation was measured at the output of the lock-in amplifier V_Ω', which was not fed into the HV (as would be the case in closed loop operation) but into a chart recorder. A peaklike signal response appears first at the lock-in output (Fig. 5) due to the sudden phase change produced between the interference pattern and the already recorded hologram. Next this signal rapidly decays to the almost zero base line because of erasure and recording of a new hologram in this new setup equilibrium position. Note that the equilibrium position means that $\psi = 0$ and consequently $V_\Omega = 0$ in Eq. (21), but erasure results also in $V_\Omega = 0$ because of lack of diffraction ($\eta \simeq 0$). Knowing the PZT conversion factor, the steplike pulse V_s may be written in terms of the phase shift effect in the setup

$$\psi_f = K^0_{\mathrm{PZT}} V_s , \tag{27}$$

and substituting it into Eq. (21) we see that

$$V_\Omega \propto \sin\psi_f \simeq \psi_f \text{ for } \psi_f \ll 1. \tag{28}$$

Experimental data V_Ω vs ψ_f measured for $\psi_d = 0.12$ rad and $\alpha = 81°$ are plotted in Fig. 6 and agree with the linear relation in Eq. (28). Here α represents the angle of the polarization direction of the incident beams at the center of the crystal measured from the x axis and is defined as $\alpha \equiv \gamma_0 + [(\rho l)/2]$. The response V_Ω of the system in the open loop mode was also measured as a function of α for $\psi_d = 0.23$ rad, $\psi_f = K^0_{\mathrm{PZT}} V_s = 0.41$ rad, and $\Omega/2\pi = 3.4$ kHz. The open loop response data are displayed in Fig. 7. The value $\alpha = \pi/4$ (vertical polarization at the center of the crystal) corresponds to $V_\Omega = 0$ according to Eq. (21). The maximum absolute value for V_Ω should correspondingly be found for $\alpha = N\pi/2$ (N is an integer) as is in fact found in Fig. 7. Curves (a) and (b) in Fig. 7 correspond to the open loop operation response for a positive and negative steplike V_s pulse, respectively, representing the PZT jumping in one direction or the opposite one. All experimental data were measured using an intensity of interfering beams at the input crystal surface of $I_R(0) = I_S(0) \simeq 50$ μW/cm^2, and the spatial frequency of the hologram was ~900 lines/mm.

Under these conditions the recording time in our BTO crystal (thickness $l = 2.4$ mm) was measured to be ~2 s. The total noise in the setup, including electronics and optics at the frequency of 3.4 kHz, as measured at the lock-in output, was not higher than 0.3 μV as appears in Fig. 6 and did not vary appreciably for frequencies other than 3.4 kHz. As deduced from Fig. 6 the signal V_Ω reaches the noise level for $\psi_f \simeq 0.01$ rad (for $\psi_d = 0.12$ rad and $\alpha = 81°$). For data in Fig. 7 corresponding to $\psi_d = 0.23$ rad and choosing the situation $\alpha = 90°$ where the response V_Ω is maximum, signal level noise for $\psi_f \simeq 0.005$ rad as may be evaluated from Eq. (21). This means that for the latter operation

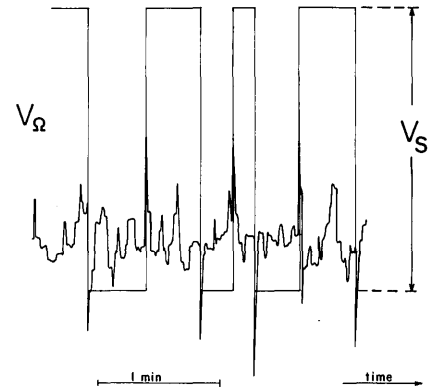

Fig. 5. Open loop operation of the stabilization system. A steplike phase shift $\psi_f = 0.41$ rad is produced in the holographic setup by an appropriate steplike voltage V_s applied at PZT. A peaklike response V_Ω' at the lock-in output results. Data in Figs. 6 and 7 were obtained in this way. Note the instability of the holographic setup resulting in a nonstable signal between peaks. The lock-in is tuned to $\Omega/2\pi = 3.4$ kHz.

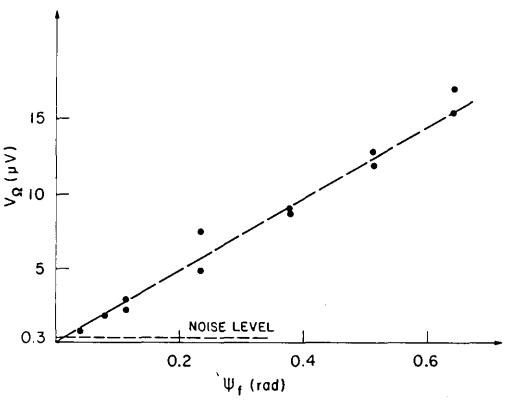

Fig. 6. Open loop response V_Ω of the stabilization system as a function of $\psi_f \propto V_s$ [Eq. (27)] for $\psi_d = 0.12$ rad, $\Omega/2\pi = 3.4$ kHz, $\alpha = \gamma_0 + \rho l/2 = 81°$, and $I_S/(I_S + I_R) \simeq 0.5$ at the input face of BTO [see Eq. (21)]. Note that the overall noise level, as measured at the lock-in output, was $\simeq 0.3$ μV.

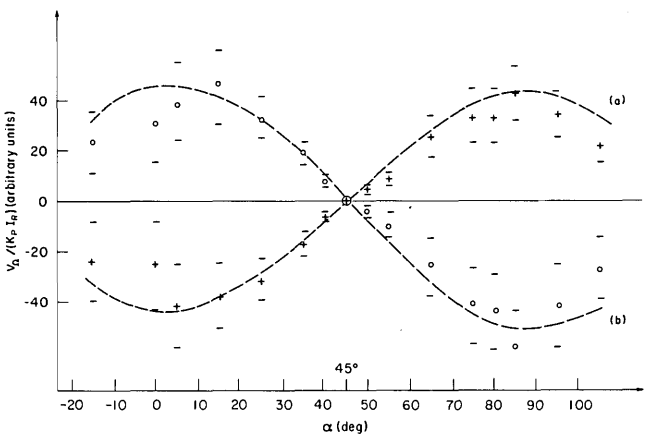

Fig. 7. Open loop normalized response $V_\Omega/K_P I_R$ as a function of the incident beam polarization angle at the center of the crystal $\alpha = \gamma_0 + \rho l/2$. $I_R = |R_0|^2 \simeq R_0 S_0$ [Eq. (21)], and K_p is a parameter characterizing the PIN diode. $\psi_d = 0.23$ rad, $\Omega/2\pi = 3.4$ kHz, $\psi_f = 0.41$ rad, and $|R_0|^2 \cong |S_0|^2$. Curves (a) and (b) indicate that the PZT was derived in one direction or the opposite, respectively.

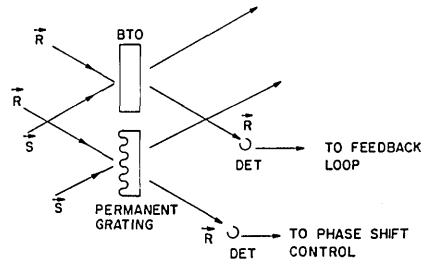

Fig. 8. Closed loop stabilizing system evaluation. The wave mixing at BTO is used to operate the stabilization system. Another part of the interfering beams is mixed using a permanent grating recorded in a positive photoresist (recorded, developed, and fixed again in its position) in this setup. The output from the permanent grating is plotted in Fig. 9. The operating conditions were similar to those reported in Fig. 7 for $\alpha = 90°$.

conditions this active stabilization system will allow phase perturbations in the setup up to a maximum of 0.005 rad. Accordingly, a maximum long-term drift of 0.005 rad/(2 s) or 0.15 rad/min may be estimated, where 2 s is the response time of our crystal.

The open loop measurements reported here are rather difficult to carry out because of the intrinsic instability of a holographic setup. In fact, these measurements should be carried out only at the moment the volume hologram recorded in the crystal is in equilibrium with the interference pattern it has been generated from [$\psi = 0$ in Eq. (21)], but there is obviously no possibility of ensuring this condition because the feedback loop is not closed. For overcoming these difficulties the open loop V_Ω signal was monitored, and a V_s pulse was applied only when V_Ω was stable and near zero indicating the system was not far from $\psi = 0$.

The actual performance of the stabilization system was compared with the predicted one as deduced from measurements in the open loop mode. For doing so, the crystal was used for operating the closed loop feedback system, and the absolute interference pattern phase shift was simultaneously measured by using a permanent grating previously recorded in a positive photoresist film. One part of the interfering beams was mixed using the crystal for operating the stabilization system, and another part was mixed using the permanent grating for absolute phase shift measurement as shown in Fig. 8. The beams mixed at the permanent grating are detected at an independent PIN diode followed by another lock-in amplifier (also tuned to 3.4 kHz similar to the one used for feedback) whose output was recorded in Fig. 9. The time evolution of this signal shows a short-term stabilization effect with a 0.2-rad oscillation instead of the 0.01 rad (peak-to-peak) that was predicted from open loop measurements. In spite of this fact, the comparatively good performance of the short-term stabilization effect may be appreciated by comparing curves *a* and *b* in Fig. 9 showing the signal evolution with and without feedback operation, respectively. From the point of view of long-term drift the system showed a somewhat low performance (36° in 1-min operation reported in Fig. 9) compared to predictions (0.15 rad or 9° maximum in 1 min).

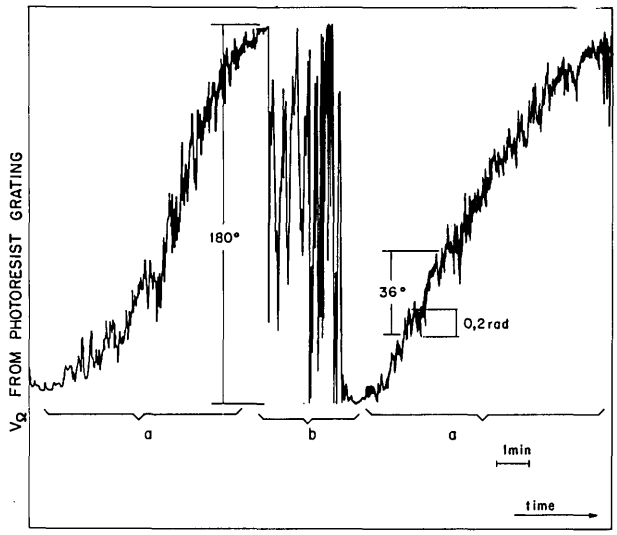

Fig. 9. Time evolution of the response V_Ω as measured in the *R*-direction mixed beam intensity at the photoresist grating in Fig. 8. It allows checking the phase shift between the interference pattern and a fixed reference grating. Note the large phase instability (fluctuations in180° or more) without feedback operation (curve *b*). In a closed loop mode (curve *a*) short-term fluctuations are strongly reduced down to 0.2-rad amplitude oscillation. A long-term drift may be appreciated (an ~36° shift occurs in a 1-min operation), which is higher than the predicted value.

We shall say finally that the lock-in amplifier in the feedback loop was operating with an integration time of 0.3 s, which represents an equivalent time delay in the feedback operation. This delay together with real-time recording characteristics of our BTO crystal are probably responsible for some features severely limiting our stabilization system performance. The 0.3-s delay in feedback loop is probably responsible for the short-term oscillating behavior of much larger amplitude than should be predicted from open loop measurements, as already reported. Such oscillations of ~0.3 s in period were indeed detected in the voltage driving the PZT in the closed-loop mode.

On the other hand, this 0.3-s time delay is not negligible compared to the crystal erasure time of 2 s. This means that a non-negligible erasure may occur during this 0.3-s delay, which is probably responsible for the somewhat poorer long-term drift performance of the feedback system compared to the predicted value. Independent measurements of the diffraction efficiency of holograms recorded in BTO during closed loop operation showed indeed the existence of diffraction efficiency fluctuations of ~0.3 s.

IV. Discussion

We have shown the possibility of employing a real-time recording photorefractive crystal for operating an active stabilization system for holographic setup.

Use of such a crystal for stabilization shows two main advantages over conventional methods that are directly related to their real-time recording characteristic. The first is concerned with the ability to operate the system even after a change in holographic setup.

In fact a new hologram is immediately recorded in the crystal, and the wave mixing for phase detection goes on without adjustment, which is not the case for permanent recording materials. The second advantage arises from the fact that recording and diffraction processes occur simultaneously so that each transmitted and holographically reconstructed wave front propagating in the same direction are identical except for their eventual relative phase shift. This means that the interference pattern of the mixed beams does not show interference fringes as should normally appear in permanent nonself-developed recording materials. The absence of such fringes allows collecting light from a larger area in the mixed beams for detection, thus improving the SNR at this first step in the feedback loop operation.

Two main limitations were also observed in this method. The first is concerned with the source of noise arising from laser light intensity fluctuations. This noise is proportional to the nonmodulated I_R^0 term (dc term) in Eq.(17). This term depends on the polarization direction of the interfering beams [the cos $(2\gamma_\rho + \rho l)$ factor in Eq. (18)], and it may be minimized by adequately choosing the γ_0 angle. If detection is performed in the R-beam direction (Fig. 3), the dc term is minimum and noise is also for $2\gamma_0 + \rho l = (2N + 1)\pi$. The same occurs for $2\gamma_0 + \rho l = N2\pi$ if detection is carried out in the S-beam direction. Note also that the modulated term in Eqs. (17)–(19) (which is our detection signal) grows with increasing diffraction efficiency η of the recorded hologram, while the dc term correspondingly decreases. That means that the SNR may be also increased by improving the diffraction efficiency of the crystal. The second limitation is concerned with the high sensitivity (short recording or erasure time) of these crystals. In fact the lower the recording/erasure time the higher the maximum allowable long-term drift, as already deduced. The response time of the crystal should also be large enough compared to the feedback electronics response in order not to allow a significative erasure in the crystal that would deteriorate the overall performance of the stabilization system. A better long-term performance may be expected by operating BTO crystal in conditions where it should exhibit lower sensitivity (red light, lower interfering beams intensity) and adjusting electronics to work with lower integration times than our reported 0.3 s, in which case a higher controlling modulation frequency Ω at the piezoelectric should certainly be necessary too.

The integration time of the lock-in amplifier introducing a delay in the feedback loop is responsible for two additional limitations not related to the crystal itself. In fact a delay in any negative feedback loop system severely limits the amplification that may be used before a positive feedback (oscillatory behavior) occurs, thus limiting the size of the external perturbations the systems may cope with. The short-term oscillations of 0.2-rad amplitude and 0.3-s period are certainly related to this fact. Besides, the integration time delay also limits the high-frequency response of the stabilization system. A higher limit should be achieved by adjusting electronics for a lower integration time.

This work should be considered as a first attempt at using real-time recording photorefractive crystals for stabilization of a holographic setup. Results are not definitely conclusive, but the method seems highly promising. Our preliminary experimental results allow as to point out some of the principal advantages and limitations of this system and show the necessity of optimization of the parameters of the crystal and the use of an adequate electronics and carefully chosen detection conditions. We remark that in spite of the fact that the absorption of BTO for the 514-nm line is far from negligible, absorption was not considered at all in our analysis for the sake of clearness.

This work was supported by CNPq (Brazilian National Council for Science and Technology Development), the Academy of Science of the U.S.S.R., FAPESP (São Paulo State Foundation for Scientific Research). The authors are very grateful to V. V. Prokofiev (IOFFE Institute, Leningrad, U.S.S.R.) for the high-quality $Bi_{12}TiO_{20}$ crystal he produced thanks to which this work was possible.

References

1. D. B. Neumann and H. W. Rose, "Improvement of Recorded Holographic Fringes by Feedback Control," Appl. Opt. **6**, 1097 (1967).
2. D. R. MacQuigg, "Hologram Fringe Stabilization Method," Appl. Opt. **16**, 291 (1977).
3. S. Johansson, L.-E. Nilsson, K. Biedermann, and K. Kleveby, "Holographic Diffraction Gratings with Asymmetric Groove Profiles," in *Proceedings, Conference on Applications of Holography and Optical Data Processing, Jerusalem Aug. 1976* (Pergamon, New York, 1976), p. 521.
4. R. C. Weyrick, *Fundamentals of Automatic Control* (McGraw-Hill, New York, 1975), Chap. 6.
5. D. von der Linde and A. M. Glass, "Photorefractive Effects for Reversible Holographic Storage of Information," Appl. Phys. **8**, 85 (1975).
6. J. P. Huignard and F. Micheron, "High-Sensitivity Read-Write Volume Holographic Storage in $Bi_{12}SiO_{20}$ and $Bi_{12}GeO_{20}$ Crystals," Appl. Phys. Lett. **29**, 591 (1976).
7. A. Marrakchi, J. P. Huignard, and P. Gunter, "Diffraction Efficiency and Energy Transfer in Two-Wave Mixing Experiments with $Bi_{12}SiO_{20}$ Crystals," Appl. Phys. **24**, 131 (1981).
8. D. L. Staebler and J. J. Amodei, "Coupled-Wave Analysis of Holographic Storage in $LiNbO_3$," J. Appl. Phys. **43**, 1042 (1972).
9. H. Kogelnik, "Coupled-Wave Theory for Thick Hologram Gratings," Bell Syst. Tech. J. **48**, 2909 (1969).
10. M. P. Petrov, S. I. Stepanov, and A. A. Kamshilin, "Light Diffraction in Photorefractive Ferroelectrics," Ferroelectrics **21**, 631 (1978).
11. J. P. Herriau, J. P. Huignard, and P. Aubourg, "Some Polarization Properties of Volume Holograms in $Bi_{12}SiO_{20}$ Crystals and Applications," Appl. Opt. **17**, 1851 (1978).
12. M. P. Petrov, S. V. Miridonov, S. I. Stepanov, and V. V. Kulikov, "Light Diffraction and Nonlinear Image Processing in Electrooptic $Bi_{12}SiO_{20}$ Crystals," Opt. Commun. **31**, 301 (1979).
13. S. I. Stepanov, T. G. Pencheva, and V. V. Kulikov, "Characteristics of Photorefraction of Cubic $Bi_{12}SiO_{20}$ Crystals," Sov. Phys. Solid State **24**, 675 (1982).